

Wave scattering among a large number of floating cylinders

Masashi Kashiwagi†

*Research Institute for Applied Mechanics, Kyushu University, 6-1 Kasuga-koen,
Kasuga-city, Fukuoka 816-8580, Japan*

(Received October 21, 2004, Accepted June 13, 2005)

Abstract. When a large number of identical cylinders are placed in an array with equal separation distance, near-resonant phenomena may occur between cylinders at critical frequencies, and cause large wave forces on each element of the array. In this paper, 64 truncated circular cylinders arranged in 4 rows and 16 columns are considered to check occurrence of near-resonant phenomena and performance of theoretical predictions based on the potential flow. Experiments are conducted in head waves to measure the wave elevation along the longitudinal centerline of the model, and measured results are compared with numerical ones. Attention is focused on the spatial variation of the wave amplitude around the first near-trapped-mode frequency.

Key words: hydrodynamic interaction; trapped mode; wave transmission; spatial distribution; truncated circular cylinders.

1. Introduction

For the development of column-supported very large floating structures to be used as a floating airport or an artificial island, wave interactions among a great number of cylinders must be understood and predicted accurately. With the linear potential-flow assumption, several versions of the wave interaction theory are available at the present time (for a recent review, the reader is referred to Newman 2001).

The author has developed a computer code combining a quadratic isoparametric boundary element method for computing the diffraction characteristics of an elementary body of general geometry and Kagemoto and Yue's (1986) interaction theory among many bodies. This code has also been extended to the hierarchical scheme (Kashiwagi 2000), which enables us to treat the wave interactions among a great number of columns with order of several thousands. Using these calculation methods, we can predict the wave field around and resulting wave forces on individual floating bodies. A number of papers have been published (e.g. Kagemoto *et al.* 1998), showing comparisons of the wave amplitude between measured and computed results. However those comparisons are made at certain limited points of a simple arrangement of bodies, and thus it is rather difficult to imagine the overall spatial distribution of a complicated wave field.

† Professor, E-mail: kashi@riam.kyushu-u.ac.jp

Another topic related to the present paper is the phenomena of near-trapped waves to be observed for periodically-arranged many cylinders, discussed by Maniar and Newman (1997). It is pointed out that the wave amplitude will be very large at near-trapped-mode frequencies and the linear potential-flow predictions are rather poor around these frequencies (Kagemoto *et al.* 2002). However, this should be checked more thoroughly through comparison between reliable measurements and accurate numerical computations.

In this paper, experiments are conducted using a model consisting of 64 equally-spaced vertical circular cylinders (an array of 4 rows times 16 columns), and waves are measured at a large number of frequencies including the first near-trapped-mode frequency of Neumann type and at 32 positions separated equally along the centerline of the tested model. Then the measured results are compared with corresponding numerical results by the wave interaction theory. It is shown that the overall quantitative agreement is very good, but when the wave amplitude becomes large due to wave resonant phenomena, numerical results obviously tend to be larger than measured ones.

2. Calculation method

2.1 Formulation

As shown in Fig. 1, a structure supported by a large number of columns is considered. The geometry of an elementary column considered here is a truncated circular cylinder with radius a (diameter $D = 2a$) and draft d . The centerlines of adjacent cylinders are separated by a distance $2s$ in both x - and y -axes of a Cartesian coordinate system, where $z = 0$ is the plane of the undisturbed free surface and the water depth is constant at $z = h$.

Under the assumption of incompressible and inviscid flow with irrotational motion, the velocity potential is introduced, satisfying Laplace's equation. The boundary conditions are linearized and all oscillatory quantities are assumed to be time-harmonic with circular frequency ω . In accordance with the experiment which will be explained later, only the diffraction problem is considered in this paper. For the radiation problem including generalized elastic motions, the reader is referred to Kashiwagi (2000).

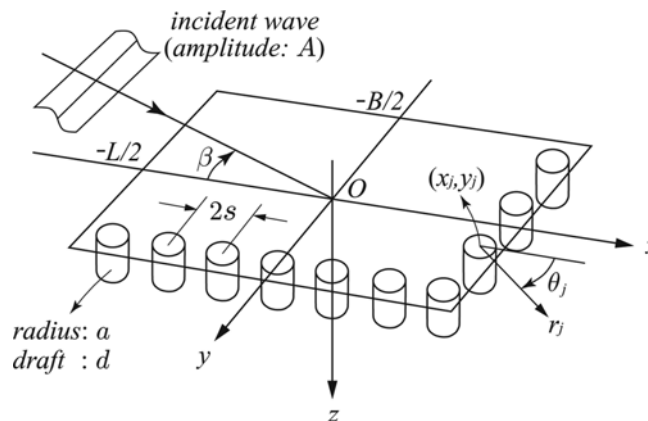


Fig. 1 Coordinate system and notations

The velocity potential for the diffraction problem is expressed in the form

$$\Phi = \operatorname{Re} \left[\frac{gA}{i\omega} \{ \phi_I(x, y, z) + \phi_S(x, y, z) \} e^{i\omega t} \right] \quad (1)$$

where g and A are the gravitational acceleration and the amplitude of an incident wave, respectively. ϕ_I and ϕ_S are the incident-wave and scattering potentials, respectively, and the sum $\phi_I + \phi_S \equiv \phi_D$ is referred to as the diffraction potential.

2.2 Diffraction characteristics of elementary body

In the wave interaction theory for a large number of bodies, ϕ_I is not necessarily a plane progressive wave, but a set of “generalized” incident waves defined in terms of a local cylindrical coordinate system (r_j, θ_j, z) of the j -th body (see Fig. 1):

$$\{ \psi_I^j \} = \left\{ \begin{array}{l} Z_0(z) J_p(k_0 r_j) e^{-ip\theta_j} \\ Z_n(z) I_p(k_n r_j) e^{-ip\theta_j} \end{array} \right\} \quad (2)$$

where $p = 0, \pm 1, \pm 2, \dots, \pm\infty$, $n = 1, 2, \dots, \infty$, and

$$\left. \begin{array}{l} Z_0(z) = \frac{\cosh k_0(z-h)}{\cosh k_0 h}, \quad Z_n(z) = \frac{\cos k_n(z-h)}{\cos k_n h} \\ \frac{\omega^2}{g} \equiv K = k_0 \tanh k_0 h = -k_n \tanh k_n h \end{array} \right\} \quad (3)$$

J_p and I_p in Eq. (2) denote the first kind of Bessel function and modified Bessel function, respectively.

Let the velocity potential of an elementary wave in Eq. (2) and the corresponding scattering potential be denoted by $\psi_I^j(x, y, z)$ and $\phi_S^j(x, y, z)$, respectively. These potentials satisfy Laplace's equation and the free-surface and sea-bottom conditions. In addition, $\phi_S^j(x, y, z)$ satisfies the radiation condition at infinity. In this case, Green's theorem gives an integral equation for the diffraction potential, $\phi_D^j = \psi_I^j + \phi_S^j$, of the form

$$C(P) \phi_D^j(P) + \iint_{S_j} \phi_D^j(Q) \frac{\partial}{\partial n_Q} G(P; Q) dS = \psi_I^j(P) \quad (4)$$

where $C(P)$ is the solid angle, $P = (x, y, z)$ is the field point, $Q = (x', y', z')$ is the integration point on the wetted surface of the j -th body S_j , and $\partial/\partial n_Q$ denotes the normal derivative with the normal vector defined as positive when directing out of the body. $G(P; Q)$ is the free-surface Green function, which can be expressed as

$$G(P; Q) = \frac{i}{2} C_0 Z_0(z) Z_0(z') H_0^{(2)}(k_0 R) + \frac{1}{\pi} \sum_{n=1}^{\infty} C_n Z_n(z) Z_n(z') K_0(k_n R) \quad (5)$$

where

$$R = \sqrt{(x-x')^2 + (y-y')^2} \quad (6)$$

$$C_0 = \frac{k_0^2}{K + h(k_0^2 - K^2)}, \quad C_n = \frac{k_n^2}{K - h(k_n^2 + K^2)} \quad (7)$$

$H_0^{(2)}$ and K_0 in Eq. (5) are the second kind of Hankel function and modified Bessel function, respectively. These functions can be recast in the series-expansion form by expressing $x + iy = r \exp(i\theta)$ and $x' + iy' = r' \exp(i\theta')$ and by using the addition theorem of Bessel functions. Considering the case of field point P in a fluid, $C(P) = 1$ and $r > r'$. Therefore, from Eq. (4) and Eq. (5), the following expression of the scattering potential may be obtained:

$$\phi_S^j(P) = \sum_{m=-\infty}^{\infty} \left[B_{m0}^j \{ Z_0(z) H_m^{(2)}(k_0 r) e^{-im\theta} \} + \sum_{n=1}^{\infty} B_{mn}^j \{ Z_n(z) K_m(k_n r) e^{-im\theta} \} \right] \quad (8)$$

where

$$\left. \begin{aligned} B_{m0}^j &= -\frac{i}{2} C_0 \iint_{S_j} \phi_D^j(Q) \frac{\partial}{\partial n_Q} Z_0(z') J_m(k_0 r') e^{im\theta'} dS \\ B_{mn}^j &= -\frac{1}{\pi} C_n \iint_{S_j} \phi_D^j(Q) \frac{\partial}{\partial n_Q} Z_n(z') I_m(k_n r') e^{im\theta'} dS \end{aligned} \right\} \quad (9)$$

A set of coefficients $\{B_{m0}^j, B_{mn}^j\}$ represents the diffraction characteristics corresponding to the elementary wave, $\psi_I^j(P)$. By considering the diffraction problems for all elementary waves in $\{\psi_I^j\}$ defined by Eq. (2) in the same manner, we can construct the matrix of the diffraction characteristics; the transpose of which is denoted as $[B_j]^T$. Then, the scattering potentials of the j -th elementary body corresponding to the generalized incident waves $\{\psi_I^j\}$ can be written in the vector form

$$\{\phi_S^j\} = [B_j]^T \{\psi_S^j\} \quad (10)$$

where

$$\{\psi_S^j\} = \begin{cases} Z_0(z) H_m^{(2)}(k_0 r_j) e^{-im\theta_j} \\ Z_n(z) K_m(k_n r_j) e^{-im\theta_j} \end{cases} \quad (11)$$

with $m = 0, \pm 1, \pm 2, \dots, \pm\infty$, and $n = 1, 2, \dots, \infty$.

2.3 Wave-body interaction theory

When the number of columns is of order more than several hundreds, the hierarchical interaction theory developed by Kashiwagi (2000) must be applied. However, the ordinary wave interaction theory (Kagemoto and Yue 1986) suffices for comparison with the experiments of 64 vertical cylinders conducted in this paper.

Let us consider the flow around the i -th body among N_B elementary columns. First the incident-wave potential incoming from the outside is expressed with a cylindrical coordinate system of the i -th body as follows:

$$\phi_I = Z_0(z) e^{-ik_0(x \cos \beta + y \sin \beta)} \quad (12)$$

$$\begin{aligned} &= \alpha_i(k_0, \beta) \sum_{p=-\infty}^{\infty} e^{ip(\beta - \pi/2)} \{Z_0(z) J_p(k_0 r_i) e^{-ip\theta_i}\} \\ &\equiv \{a^i\}^T \{\psi_I^i\} \end{aligned} \quad (13)$$

where

$$\alpha_i(k_0, \beta) = e^{-ik_0(x_i \cos \beta + y_i \sin \beta)} \quad (14)$$

with β the angle of incident wave relative to the positive x -axis and (x_i, y_i) the center of the i -th body in the global coordinate system. Note that the coefficient vector $\{a^i\}$ can be explicitly given from Eq. (13).

Incident waves impinging upon the i -th body consist of not only the incident wave given by Eq. (13) but also scattered waves from other bodies. Thus it can be written as

$$\begin{aligned} \phi_I^i &= \{a^i\}^T \{\psi_I^i\} + \sum_{\substack{j=1 \\ j \neq i}}^{N_B} \{A_S^j\}^T \{\psi_S^j\} \\ &= \left(\{a^i\}^T + \sum_{\substack{j=1 \\ j \neq i}}^{N_B} \{A_S^j\}^T [T_{ji}] \right) \{\psi_I^i\} \end{aligned} \quad (15)$$

Here $\{A_S^j\}$ is the vector of unknown coefficients of the scattering potential due to the j -th body. $[T_{ji}]$ is the coordinate transformation matrix, relating $\{\psi_S^j\}$ with $\{\psi_I^j\}$; a concrete expression of which can be given by Graf's addition theorem for Bessel functions.

The quantity in parentheses in Eq. (15) can be regarded as the amplitude vector and $\{\psi_I^i\}$ is, as defined in Eq. (2), the vector of generalized incident waves. The scattering potentials in response to $\{\psi_I^i\}$ are already obtained in the form of Eq. (10). Therefore, the scattering potential of the i -th body due to the incident wave of Eq. (15) can be expressed as

$$\begin{aligned} \phi_S^i &= \left(\{a^i\}^T + \sum_{\substack{j=1 \\ j \neq i}}^{N_B} \{A_S^j\}^T [T_{ji}] \right) [B_i]^T \{\psi_S^i\} \\ &= \{A_S^i\}^T \{\psi_S^i\} \end{aligned} \quad (16)$$

One can therefore obtain a linear set of equations for determining the vector of unknown coefficients, $\{A_S^i\}$, in the form

$$\{A_S^i\} - [B_i] \sum_{\substack{j=1 \\ j \neq i}}^{N_B} [T_{ji}]^T \{A_S^j\} = [B_i] \{a^i\}, \quad i = 1 \sim N_B \quad (17)$$

Solving Eq. (17) completes the flow field, and then the wave elevation on the free surface ($z = 0$) can be computed from Eq. (12) and Eq. (16) as follows:

$$\frac{\zeta(x, y)}{A} = \phi_I(x, y, 0) + \sum_{j=1}^{N_B} \{A_S^j\}^T \{ \psi_S^j(r_j, \theta_j, 0) \} \quad (18)$$

2.4 Numerical computations

First we need to solve the integral equation (4) for an elementary body (which is a vertical circular cylinder in the present case) and to determine the diffraction characteristics matrix $[B_i]$. For this purpose, the higher-order boundary-element method using isoparametric 9-point quadratic elements is utilized. Since a vertical circular cylinder has double symmetries with respect to the x and y -axes, only the first quadrant of a body is discretized into panels, and symmetry relations for the geometry and velocity potential are exploited. To assure high numerical accuracy, 320 panels over one quadrant were used, which was found to give completely converged results.

In computations of the interaction part, the numbers of Fourier series in the θ -direction (M) and of evanescent wave modes (N) must be finite, which depend on the arrangement of columns, the frequency, and the water depth. In the present paper, computations are performed for a model used in the experiments; that is, as shown in Fig. 2, 64 circular cylinders arranged in 4 rows and 16 columns. For this model, $M = 4$ and $N = 3$ are chosen after convergence check for $Ks = 1.0$, $\beta = 0^\circ$ and $h = 3d$, which achieved five decimals absolute accuracy. Even in this case, the number of total unknowns for $N_B = 64$ is $(2M + 1) \times (N + 1) \times N_B = 2304$. To reduce the number of unknowns and thus the computation time, double symmetry relations with respect to the x - and y -axes for the whole structure have been exploited.

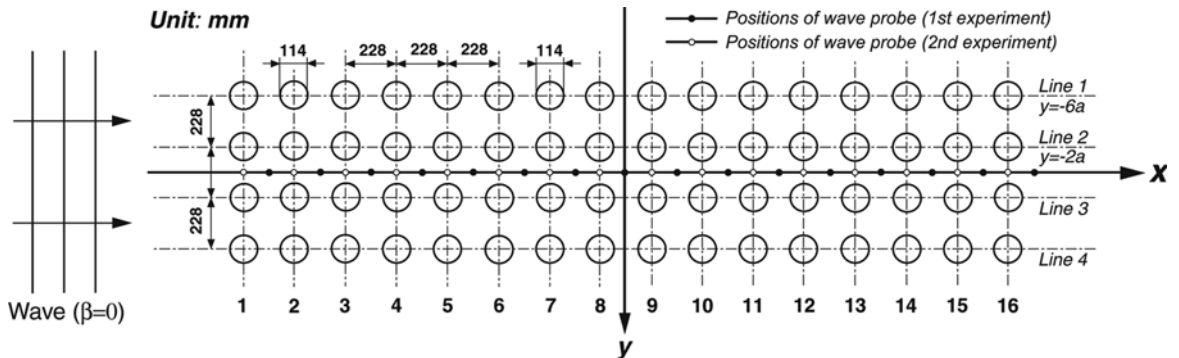


Fig. 2 Experimental model: Arrangement of 64 truncated circular cylinders fixed in head waves

3. Outline of experiments

Fig. 2 shows a model used in the experiments, consisting of 64 equally-spaced truncated circular cylinders. The diameter of an elementary cylinder is $D = 114$ mm. The separation distance between centerlines of adjacent cylinders, $2s$, was set equal to $2D$ in both x - and y -axes. To see effects of the draft of cylinders on the wave interactions, two cases of $d = D$ and $d = 2D$ were tested. The wave elevation inside the structure was measured at 32 positions along the longitudinal centerline (x -axis) using wave probes of capacitance type. (In reality, 16 wave probes separated each with $2s$ were used and measurements were performed twice by shifting the positions of wave probes by half of the separation distance, s .)

The experiments were conducted in head waves generated in Ocean Engineering Model Basin (length 65 m, breadth 5 m, water depth 7 m) of Research Institute for Applied Mechanics, Kyushu University. The steepness of regular waves (the ratio of wave height with wave length, H/λ) was set approximately equal to $1/50$. The circular frequency ω of incident wave was varied in the range of $Ks = \omega^2 s/g = 0.2 \sim 1.6$. Measured data were analyzed using an ordinary Fourier-analysis technique, from which the first-order term oscillating with circular frequency ω was extracted and stored in the form of the amplitude and phase difference. (The phase lead is defined as positive and measured from the time instant when the trough of incident wave comes at $x = 0$.)

4. Results and discussion

4.1 Frequency dependence on wave elevation

To see variation tendency of the wave elevation due to hydrodynamic interactions, measurements have been made for many different values of Ks . Because of shortage of space, only the results at 6 representative points are shown in Figs. 3-5 with Ks taken as the abscissa, which are for the case of $d = D$. The first two positions (just beside Column No. 1 and exactly between No. 1 and No. 2) shown as Fig. 3 are on the upwave side. Rapid and regular variation can be seen in the frequency range lower than $Ks \cong 1.26$, which are due to hydrodynamic interactions with waves diffracted from downstream cylinders. Although the separation distance between the first two positions is just s , the wave amplitude becomes much different as the frequency increases.

The second two positions shown as Fig. 4 are just beside Column No. 8 and exactly between No. 8 and No. 9; these are near the midst of the structure (the real midst is exactly between No. 8 and No. 9). Compared to the variation pattern at upwave positions, the amplitude variation with respect to Ks becomes mild for lower frequencies. However, at the midst (i.e., exactly between No. 8 and No. 9), the amplitude becomes very large especially when the frequency approaches $Ks \cong 1.26$ from lower frequencies. According to Maniar and Newman (1997), $Ks = 1.26$ corresponds approximately to a near-trapped mode of Neumann type. Computed results are generally in good agreement with measured values. However at frequencies slightly lower than the near-trapped-mode frequency, computations apparently overpredict; which may be attributed to the potential-flow assumption in the theory. It can be seen that nondimensional values of the measured wave amplitude are all less than 3.0. Considering that the wave steepness of incident wave was $H/\lambda \cong 1/50$, we can envisage that the wave steepness of scattered wave is $H/\lambda \cong 3/50 = 1/16.7$, which becomes close to the limit of wave breaking.

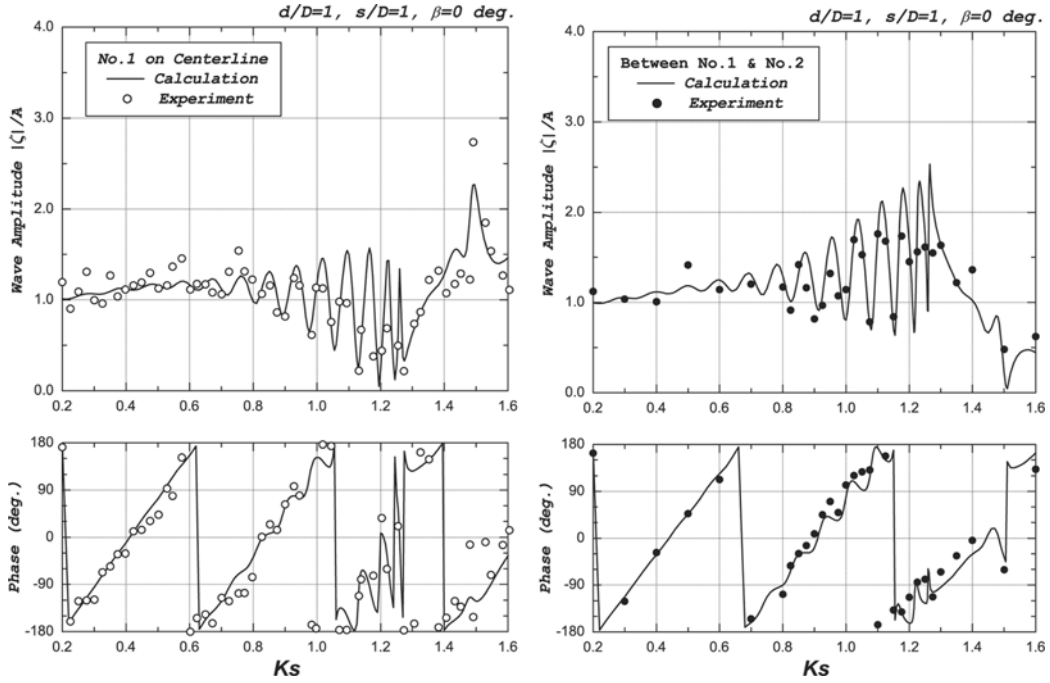


Fig. 3 Wave elevation along the centerline of the model shown in Fig. 2 at $x/a = -30$ (left figure) and at $x/a = -28$ (right figure), for the case of $d/D = 1$

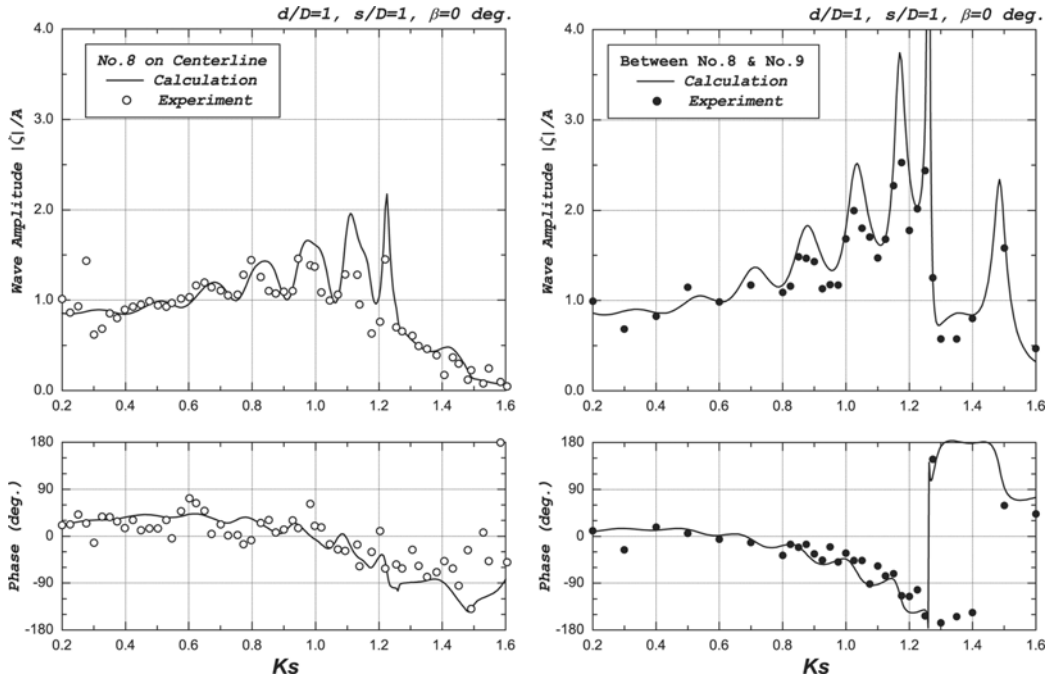


Fig. 4 Wave elevation along the centerline of the model shown in Fig. 2 at $x/a = -2$ (left figure) and at $x/a = 0$ (right figure), for the case of $d/D = 1$

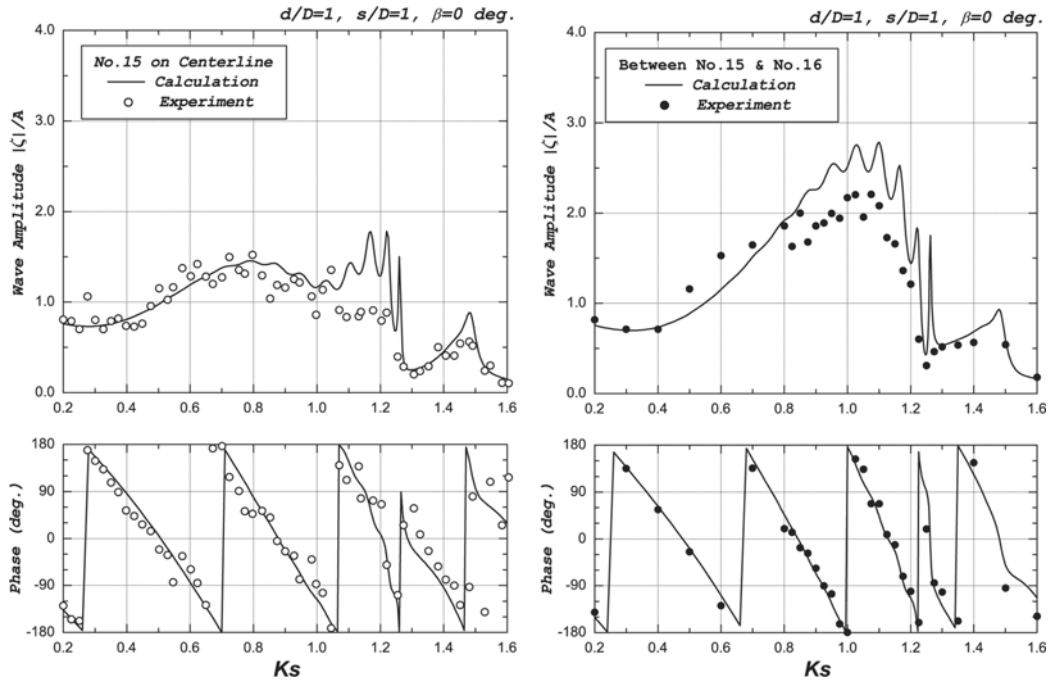


Fig. 5 Wave elevation along the centerline of the model shown in Fig. 2 at $x/a = 26$ (left figure) and at $x/a = 28$ (right figure), for the case of $d/D = 1$

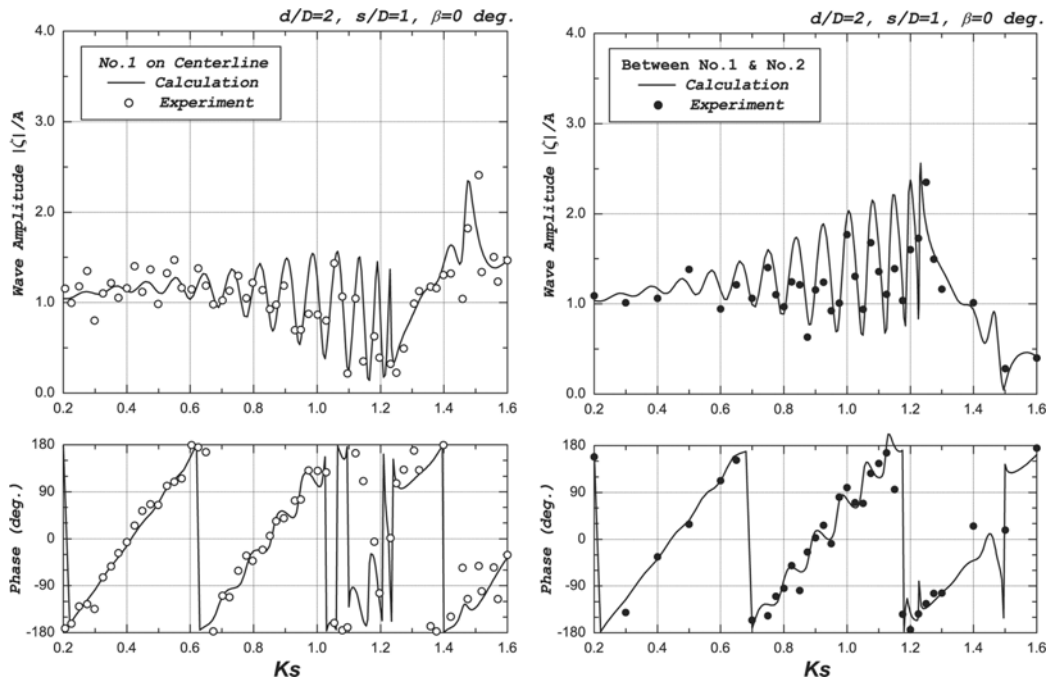


Fig. 6 Wave elevation along the centerline of the model shown in Fig. 2 at $x/a = -30$ (left figure) and at $x/a = -28$ (right figure), for the case of $d/D = 2$

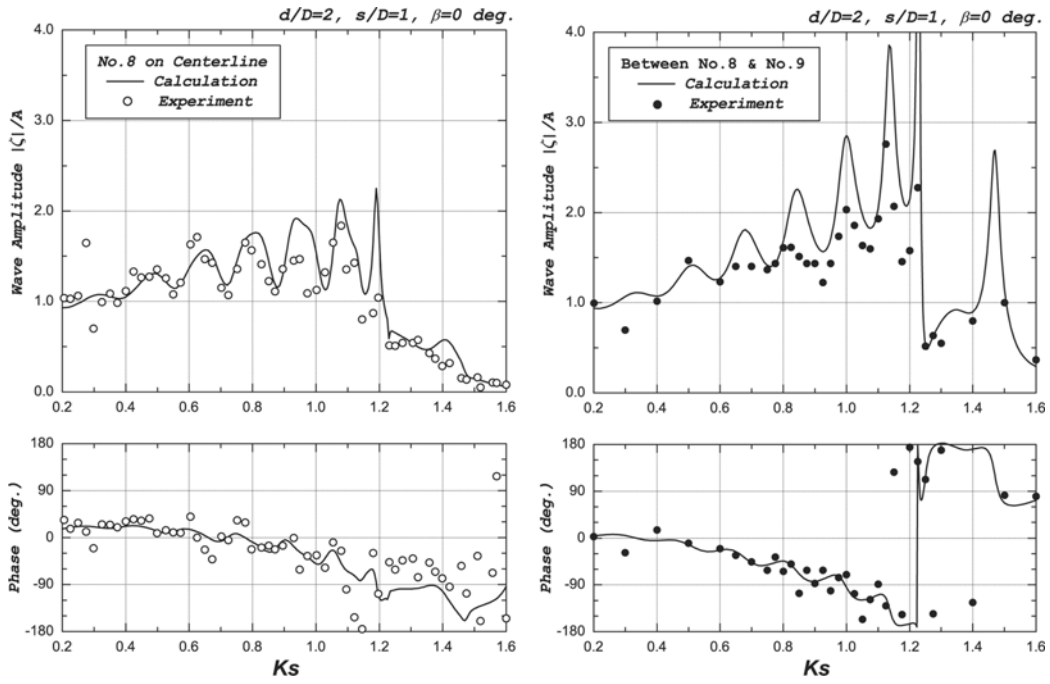


Fig. 7 Wave elevation along the centerline of the model shown in Fig. 2 at $x/a = -2$ (left figure) and at $x/a = 0$ (right figure), for the case of $d/D = 2$

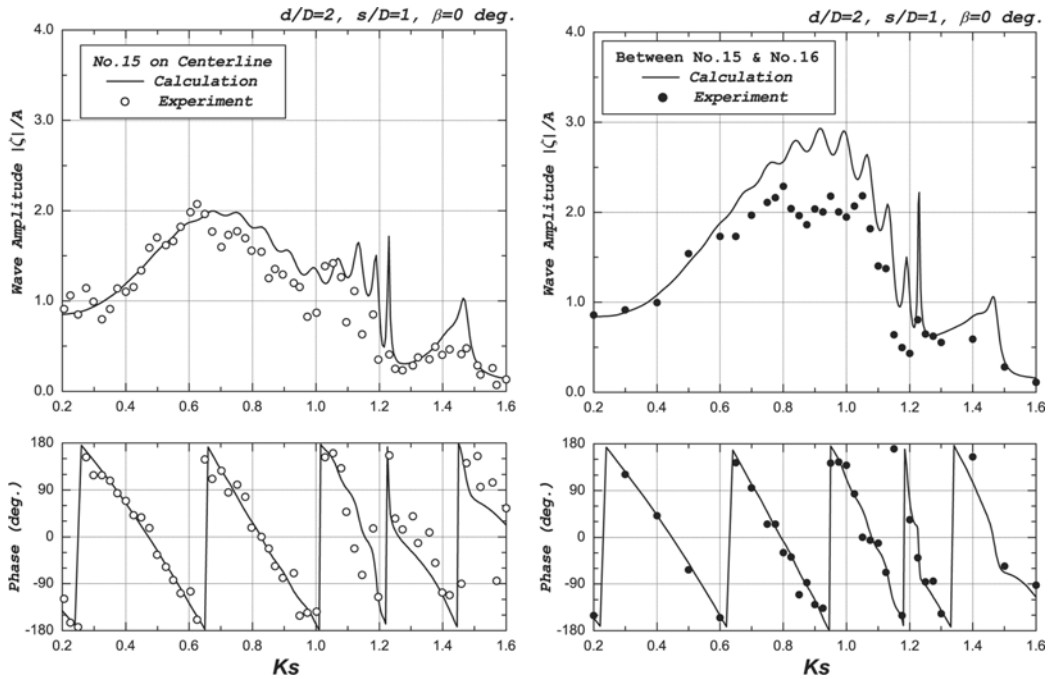


Fig. 8 Wave elevation along the centerline of the model shown in Fig. 2 at $x/a = 26$ (left figure) and at $x/a = 28$ (right figure), for the case of $d/D = 2$

The last two positions shown as Fig. 5 are just beside Column No. 15 and exactly between No. 15 and No. 16, which are on the downwave side. Variation in amplitude with respect to Ks becomes further mild. In the frequency range slightly lower than the near-trapped-mode frequency, computations predict spike-like variation, but this is not clear in measured results. Furthermore, in this frequency range, measured values are obviously lower than the computations, which may be due to effects of viscosity originating from the boundary layers of upwave cylinders. It can also be observed that the wave amplitude is much different between the two positions shown in Fig. 5, although the separation distance between these two positions is just s .

Figs. 6-8 show the results for the case of deeper draft of $d = 2D$, at the same 6 representative positions along the centerline. By comparison with Figs. 3-5, variation tendency and the degree of agreement between experiments and computations are almost the same. One noticeable and important difference is that the value of Ks corresponding to the near-trapped-mode frequency is slightly lower than that for $d = D$; that is, $Ks \cong 1.24$ for the case of $d = 2D$ whereas $Ks \cong 1.26$ for the case of $d = D$.

4.2 Spatial variation at some fixed frequencies

It has been shown that the wave amplitude varies depending on the measurement position and the wave frequency. To see spatial variation of the wave elevation, wave amplitudes along the centerline are shown in Figs. 9 and 10, with positions along the centerline taken as the abscissa. Fig. 9 is the case of $d = D$ and includes the results for eight cases of $Ks = 0.8, 1.0, 1.1, 1.15, 1.2, 1.3, 1.4$ and 1.5 . On the other hand, Fig. 10 is for the case of $d = 2D$ and $Ks = 0.8, 1.0, 1.05, 1.1, 1.15, 1.2, 1.25$ and 1.3 .

First it can be seen that variation characteristics for two cases of $d = D$ and $d = 2D$ are very similar except that the near-trapped-mode frequency is slightly different. Computations have been performed at regular intervals of 201 points along the centerline and shown by a continuous solid line. The results in the first measurements are shown with closed circles (\bullet), which correspond to the values measured at middle positions between the cylinders shown in Fig. 2. Shown by open circles (\circ) are the results in the second measurements at positions just beside the cylinders.

As the position goes downstream, the maximum of wave amplitude increases at lower frequencies, e.g. $Ks = 0.8$ to 1.1 . Furthermore, the envelope of wave amplitude begins to fluctuate, as the frequency increases up to the near-trapped-mode frequency ($Ks \cong 1.26$ for $d = D$ and $Ks \cong 1.24$ for $d = 2D$). In fact, the number of crests in the envelope of amplitude variation decreases as the frequency approaches the near-trapped-mode frequency. Variation tendency changes drastically when the frequency becomes higher than the near-trapped-mode frequency. When the amplitude variation is large, the wave amplitudes at points just beside cylinders are relatively small, and on the contrary the values at middle points between cylinders are large; this is actually a typical wave pattern at near-trapped modes.

Regarding the degree of agreement between experiments and numerical computations, the overall agreement is good and variation tendency is well predicted by the present computations. However, when the amplitude variation is large due to strong hydrodynamic interactions, numerical results obviously overpredict, which may be, as already discussed regarding Figs. 3 to 8, attributed to viscous effects not included in the present computations.

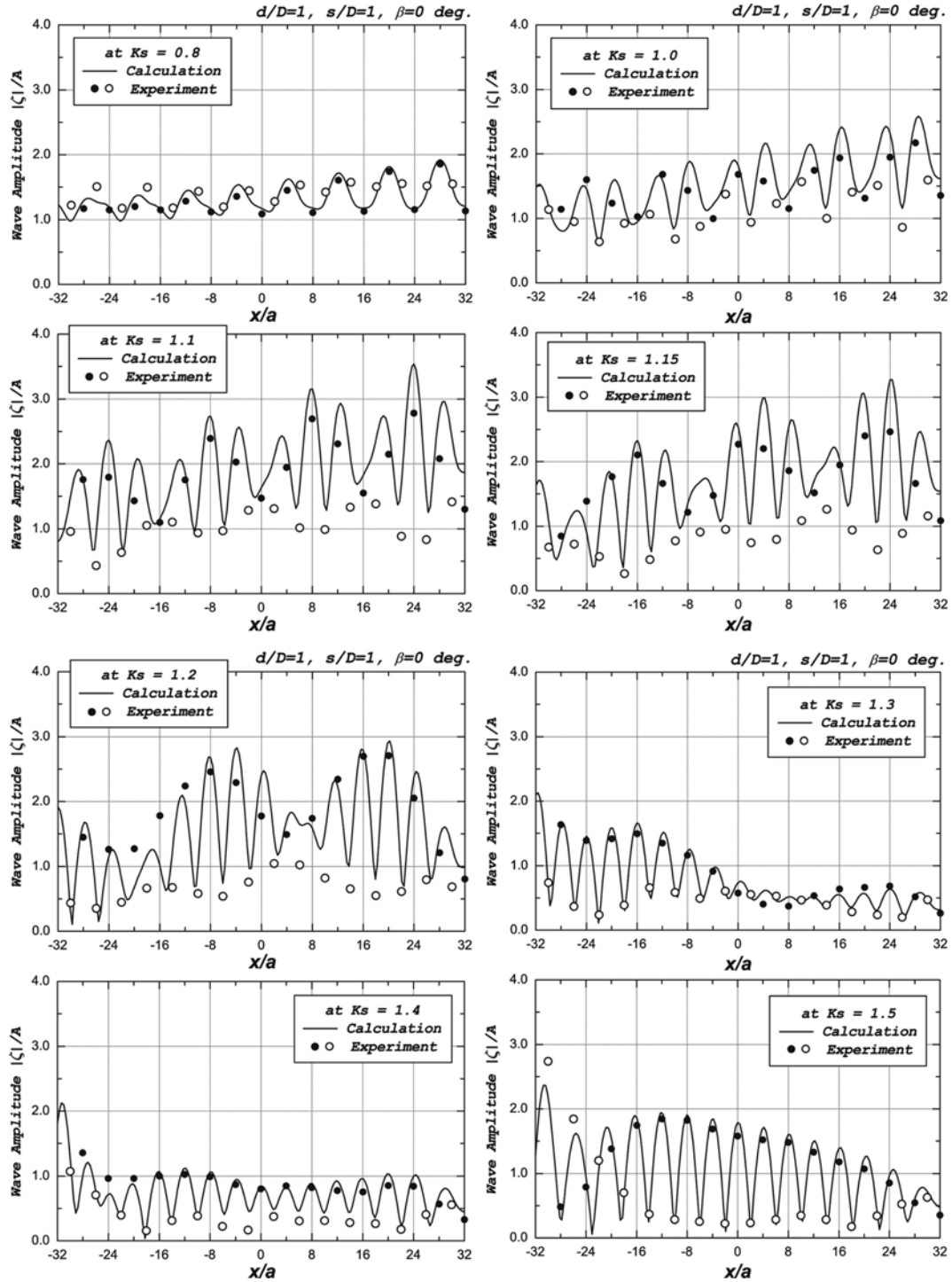


Fig. 9 Spatial variation of the wave amplitude along the centerline of the model shown in Fig. 2, for the case of $d/D = 1$

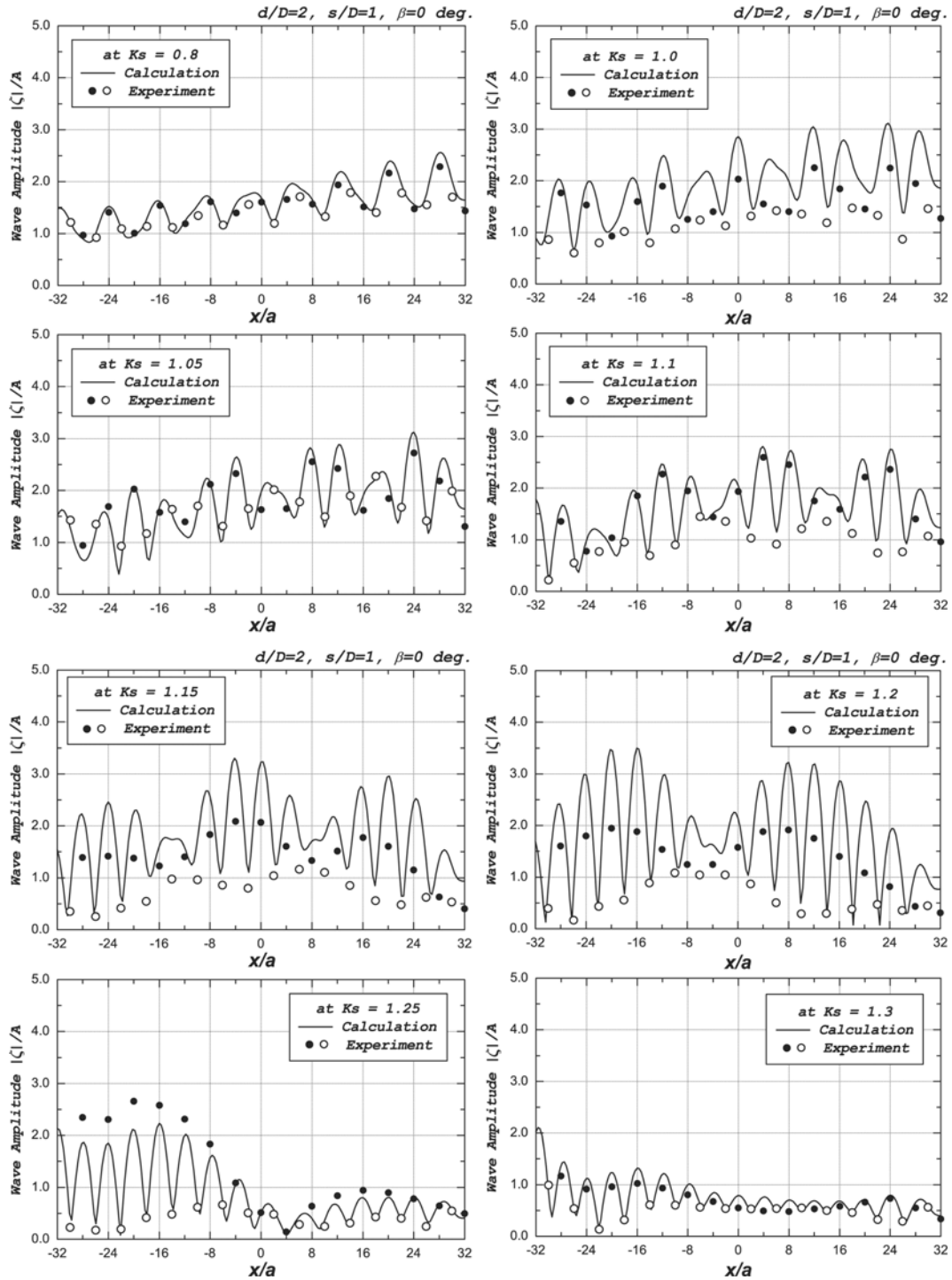


Fig. 10 Spatial variation of the wave amplitude along the centerline of the model shown in Fig. 2, for the case of $d/D = 2$

5. Conclusions

To have clear understanding on wave interactions among a great number of columns, wave measurements have been conducted at a large number of frequencies and at 32 positions along the longitudinal centerline of a model composed of 64 vertical circular cylinders periodically placed in 4 rows and 16 columns. The results were compared with numerical computations done by a combination of the quadratic boundary-element method for evaluating the diffraction characteristics of an elementary body and Kagemoto and Yue's wave interaction theory for multiple bodies.

Occurrence of the near-trapped mode was confirmed for the 64-column model used in the present study, and the near-trapped-mode frequency was found to be slightly different depending on the draft of columns. Around this near-trapped-mode frequency, variation in wave amplitude is very large, and the amplitude tends to be maximal at positions exactly between adjacent cylinders and minimal at positions just beside cylinders; which is a typical wave pattern at near-trapped modes of Neumann type.

The overall quantitative agreement was favorable between measured and computed results, and variation tendency in the wave amplitude with respect to the frequency and the spatial position was also well predicted by the present calculation method. However when the wave amplitude is very large due to near-trapped-wave phenomena, numerical results were obviously larger than measured ones.

References

- Kagemoto, H. and Yue, D.K.P. (1985), "Interactions among multiple three-dimensional bodies in water waves: An exact algebraic method", *J. of Fluid Mechanics*, **166**, 189-209.
- Kagemoto, H. and Fujino, M. *et al.* (1998), "On the wave decay around a very large semisubmersible type floating structure (2nd Report)", *J. of the Society of Naval Architects of Japan*, **184**, 271-282.
- Kagemoto, H., Murai, M., Saito, M., Molin, B. and Malenica, S. (2002), "Experimental and theoretical analysis of the wave decay along a long array of vertical cylinders", *J. of Fluid Mechanics*, **456**, 113-135.
- Kashiwagi, M. (2000), "Hydrodynamic interactions among a great number of columns supporting a very large flexible structure", *J. of Fluids and Structures*, **14**, 1013-1034.
- Maniar, H.D. and Newman, J.N. (1997), "Wave diffraction by a long array of cylinders", *J. of Fluid Mechanics*, **339**, 309-330.
- Newman, J.N. (2001), "Wave effects on multiple bodies", *Hydrodynamics in Ship and Ocean Engineering*, edited by M. Kashiwagi, RIAM, Kyushu Univ., 3-26.